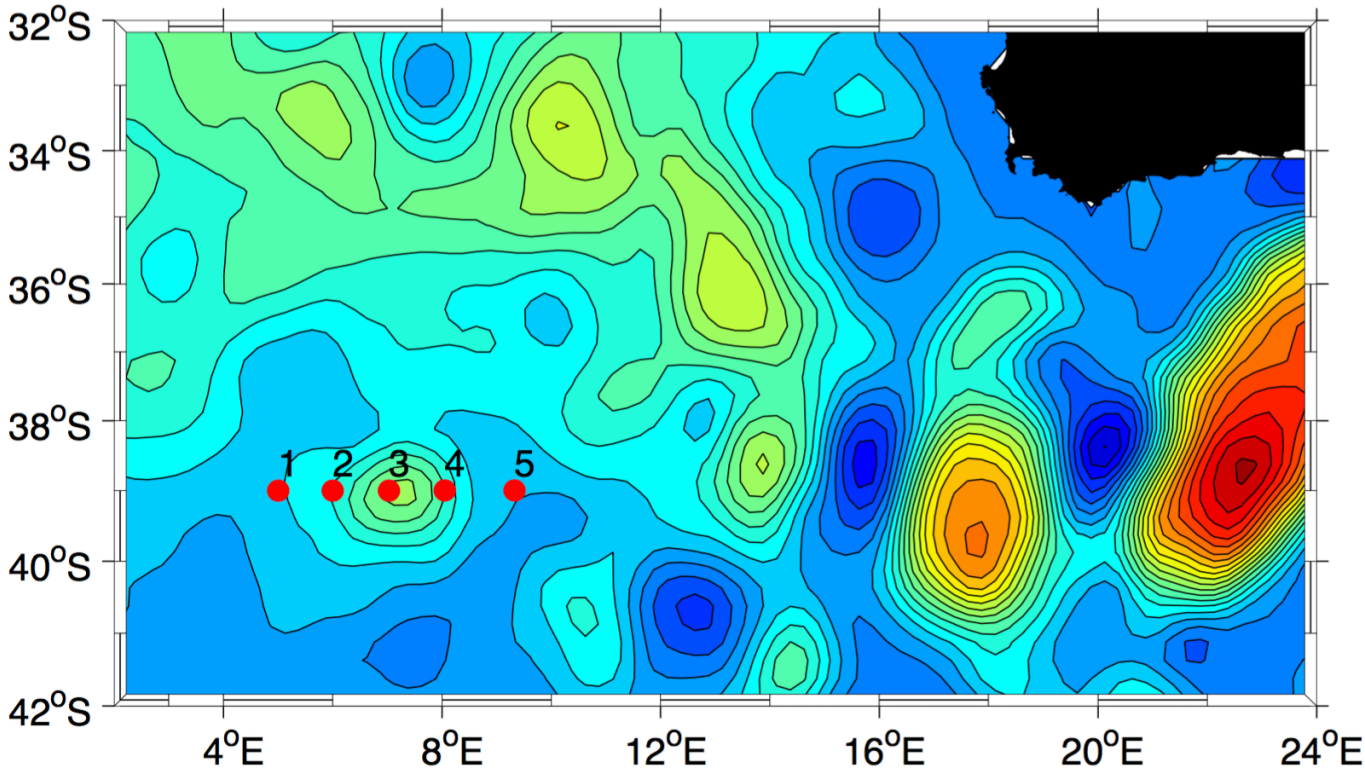

Trabajo Final de Máster:

CHARACTERISTICS OF AN AGULHAS RING

Maria Casanova Masjoan

2015/2016

Tutores: Alonso Hernández Guerra
Antonio Martínez Marrero
Pablo Sangrà Inciarte
Diana Grisolía Santos

ULPGC

FACULTAD DE CIENCIAS DEL MAR
UNIVERSIDAD DE LAS PALMAS DE GRAN CANARIA

IOCAG Instituto de Oceanografía y Cambio Global

Master Interuniversitario en Oceanografía

Final Master Work

Characteristics of an Agulhas Rings

Final master work presented by Maria Casanova Masjoan to obtain the title of the Interuniversity Oceanography Master from the University of Las Palmas de Gran Canaria.

Directed by: Professor Alonso Hernández Guerra, Dr. Antonio Martínez Marrero, Dr. Pablo Sangrà Inciarte and Dr. Diana Grisolía Santos, Department of Physics, University of Las Palmas de Gran Canaria, Instituto de Oceanografía y Cambio Global (IOCAG).

Tutors:

Alonso Hernández Guerra	Antonio Martínez Marrero	Pablo Sangrà Inciarte	Diana Grisolía Santos

Student:
Maria Casanova Masjoan

LAS PALMAS DE GRAN CANARIA
JUNE 2016

Table of contents

Abstract

Hydrographic data, SSH from altimetry, thermosalinometer and drifters measurements were acquired along an Agulhas ring during March 2010. Hydrographic survey and drifters deployment were done 5 months after the ring formation. The ring is clearly visible from altimetry and salinity from thermosalinometer data since the surface properties in the core are different from those of the surrounding waters. The structure observed with a high geostrophic velocity of 30 cm s^{-1} and mass transport of 28 Sv in the surface layers, which shows a counterclockwise rotation. The trajectory is northeastward with a translation speed of 13 cm s^{-1}, a rotating period of 8 days and a mean radius of 140 km.

1. Introduction

The southern part of Africa is a unique combination of Western Boundary Currents (WBC), the Agulhas Current, and mesoscale activity (Biastoch and Krauss, 1999; Garzoli et al., 1999). Most of the Indian Ocean leakage into the Atlantic, about 25% of the Agulhas water, takes place in the Agulhas retroflection (15-20ºE), where Agulhas rings and cyclones are generated by loop occlusion. These rings are transported through the Benguela Current forming the warm and salty upper water layer that flows northward towards the subpolar North Atlantic as the upper limb of the Meridional Overturning Circulation (MOC) in compensation for the colder southward flowing North Atlantic Deep Water (Biastoch et al., 2008; Gordon and Haxby, 1990; Richardson et al., 2003). About 9 rings per year spin off the retroflection and between 5-6 pass through the Atlantic Ocean (Biastoch and Krauss, 1999; Gordon and Haxby, 1990; Richardson, 2007). Leakage transport of the rings into the Atlantic and specifically into the Benguela Current is approximately 15 Sv (1Sv= 10^9 kg s^{-1}) (Garzoli et al., 1999; Richardson, 2007). That transport approximately compensates the about 17 Sv of NADW formed at high latitudes in The North Atlantic (Rahmstorf and England, 1997; Toggweiler and Samuels, 1995). The difference is related to the uncertainties of these transports (Hernández-Guerra et al., 2014) The Agulhas region is characterized by a high interanual and intraseasonal variability (Biastoch et al., 2008). A little variations in the Agulhas leakage may play an important role in glacial terminations, the timing of interhemispheric climate change and in the MOC (Richardson et al., 2003).

The large anticyclonic rings formed in the Agulhas retroflection translate far from the formation area, with a lifetime between 2 and 4 years and a mean diameter in the range of 200-400 km (Biastoch and Krauss, 1999; Garzoli et al., 1999). In the retroflection, smaller cyclones are also formed drifting westwards, remaining close to the retroflection and with a shorter lifetime (Biastoch and Krauss, 1999; Garzoli et al., 1999; Gordon and Haxby, 1990; Richardson, 2007). Most of the cyclones are transported southward to the South Atlantic Current and return to the Indian Ocean. Moreover, they do not translate as far as the anticyclones do. Newly formed Agulhas rings are the most energetic eddies of the world (Richardson, 2007). These rings move faster in deeper regions and slower in shallower ones (Garzoli et al., 1999). The motion of the rings is due to a positive combination of advection in the mean flow and self-induced motion (McDonagh et al., 1999).

Most of rings enter in the Brazil Current after a 2.5 year of transatlantic journey (Gordon and Haxby, 1990). Mean ring depth is 1500-2000 m, therefore contains surface, thermocline and intermediate waters (Biastoch and Krauss, 1999; McDonagh et al., 1999). The transport of the rotating water flowing with the rings is about 20-30 Sv (Gordon and Haxby, 1990). Mean northward propagation rate is in the range of 4.4 cm s^{-1} (158.4 m d^{-1}) and 8.3 cm s^{-1} (298.8 m d^{-1}) calculated with a GEOSAT track and from float data (Gordon and Haxby, 1990; Richardson, 2007).

Our analysis consists in a combination of satellite altimetry, CTD data and two NOAA drifters to characterize an Agulhas ring surveyed in March 2010. Water masses, geostrophic velocities and mass transport are calculated from CTD data. Altimetry imagery is used to identify the ring and its formation, measure its diameter and calculate the propagation rate. Finally, the drifters are used to obtain the trajectory, the period and the mean radius while the drifters remain on the ring.

The paper is organized as follows. In section 2, we present the data collection. Section 3 presents the results in different subsections. Sections 3.1 and 3.2 describe the results obtained from CTD data. In section 3.3 and 3.4 altimetry and drifters observations are showed respectively. In section 4 we present our discussion and conclusions.

2. Data collection and methods

Our data includes CTD (Conductivity-Temperature-Depth), altimeter data form AVISO and satellite-tracked surface drifting buoy. CTD data were collected during the oceanographic cruise MOC2-Austral aboard R/V Hespérides from February 8 to March 10, 2010 in the south Atlantic, along a transect starting at Ushuaia and ending in Cape Town.

For this study, we have selected data from 5 hydrographic stations in an Agulhas Ring. Measurements also includes alkalinity, pH and nitrates as obtained from water samples. Fig. 2.1 depicts the location of the hydrographic stations and the near surface zonal salinity across those stations as obtained from the onboard termosalinograph. Surface salinity clearly shows a local maximum of 35.6, which is the signal of an Agulhas Ring as indicated by a core of highest salinity. Drifter data set where obtained from 2 NOAA drifters of the Global Drifter Program, 89771(drifter 1) and 89772 (drifter 2) drogued at 15 m depth and deployed at hydrographic stations 3 and 4, respectively.

Geostrophic velocity and transport are inferred from the thermal wind equations in order to obtain the geostrophic flow in the ring. As level of no motion, we have selected the neutral density surface of γ^n=28.11 kg m^{-3}, about 2000 m depth. Neutral surface density layers of Ganachaud (2003) are adopted to divide the mass transport.

Rotatory wavelet analysis is used to infer the ring rotating rate as obtained from the components of the velocity field (Sangrà et al., 2005; Torrence and Compo, 1998). Wavelet transform is a windowing technique that enable us to adapt the frequency domain to our time intervals (Thomson and Emery, 2014). This method transforms a time series in a group of functions $g_{a\tau}(t) = g(t{:}\,\tau, q)$, derived from a mother function:

$$g_{a\tau}(t) = \frac{1}{\sqrt{a}} g[a^{-1}(t-\tau)] \qquad \text{E 2.1}$$

Where τ (real) is the translation parameter which corresponds to the central time series point of the wavelet and a (real and positive) is the scale dilation parameter which corresponds to the width of the wavelet (Thomson and Emery, 2014).

$$g(t) = e^{-t^2/2} e^{+i\omega t} \qquad \text{E 2.2}$$

In addition, from our two drifters data different proporties of the ring, like center trajectory, mean radius and its period can been calculated following Brassington (2010) and Grisolía-Santos et al. (2015) It is based on that drifting buoys inside ocean eddies exhibits Lagrangian trajectories that orbit the local extremum in geopotential, so then, points along the eddy boundary, assuming that vary smoothly on time, can be estimated at any time. The mean buoy drift is calculated assuming that the lagrangian trajectory of the buoy inside the eddy have an oscillatory motion. The method is used only with data obtained when the drifter is inside the ring. To remove inertial oscillations, data are filtered using a low-pass butterworth filter with a cut-off frequency of 0.0278 h^{-1}. Therefore, plotting each orthogonal coordinate versus time we can obtain the maximum and minimum extremes points for an orbit and thus, the northern/southern and Eastern/western points of the trajectories. Interpolating these extremes for each instant of time with a cubic spline and averaging them allow us to obtain the eddy center trajectory (Fig. 2.2). From the interpolate extremes we could then obtain the radius and the period for each time. In addition, we have obtained the loops of the drifters inside the rings from the orbits calculated.

3. Results

3.1. Ring signature in the hydrographic fields

Vertical sections of potential temperature, neutral density, salinity, pH and nutrients, from surface to 2000 m depth, and θ/S diagram are used to identify water masses (Figures 3.1 and 3.2). The decrease on the inclination of γ^n isolines tilting with depth until becoming almost flat at γ^n=27.75 kg m^{-3} indicates the depth rings is about 2000 m. Thus, we choose as no motion level in the flat isopycnal of γ^n =28.11 kg m^{-3}.

In the vertical sections and the θ/S diagram we compare those stations located at the periphery of the ring (stations 1 and 5) with those located inside the ring (stations 2,3 and 4). The signature of the ring is revealed by a warmer and saltier water mass core of Indian Ocean origin identified as Agulhas Water (AGW) in the surface and subsurface layers

with $\gamma^n \leq 26.5$ kg m^{-3} and salinity of 35.5. This contrast with the colder and fresher Atlantic Surface Water (ASW) found at the periphery stations with a salinity of about 34.8. There is also a distinct signature for central water from surface to density layers of $\gamma^n \leq 27.1$ kg m^{-3} (about 750 m depth), which define the thermocline layer with $6 \leq \theta \leq 16$ ºC. South Atlantic Central Water (SACW) is observed inside and outside the ring. Below this water mass, 27.1 kg $m^{-3} \leq \gamma^n \leq 27.4$ kg m^{-3} and $\theta \leq 6$ ºC, are found the intermediate waters where Antarctic Intermediate Water (AAIW) dominates, with salinity values of 34.1, and traces of Red Sea Water (RSW) of grater salinity, 34.3, coming from the Agulhas Current (van Aken et al., 2003). Above the intermediate water, North Atlantic Deep Water (NADW) is present ($\gamma^n \leq 27.9$ kg m^{-3}). At the bottom we find Antarctic Bottom Water (AABW) ($\gamma^n \geq 27.9$ kg m^{-3}). In the last two water masses the Agulhas ring signal is not apparent (Fig, 3.1).

3.2. Geostrophic velocities and mass transport

The reference level to integrate the thermal wind equations has been chosen as the neutral density interface at $\gamma^n = 28.11$ kg m^{-3} (about 2000 m), where the ring signal is not apparent. The water column is divided into 14 density layers following Ganachaud (2003). Geostrophic velocity as function of depth along the ring is shown in Figure 3.3. Maximum surface velocities are found in stations 2-3 and 4-5, about 30 cm s^{-1}, being the positive/negative values northward/southward directions. From almost 2000 m depth to the bottom, the geostrophic velocity is approximately zero.

Figure 3.4a shows the mass transport per density layer integrating the complete section. Positive sign means northward transport. There is a net integrated mass transport to the north, being the greatest transport near the surface with 1.2 Sv. There is no transport below $\gamma^n = 28.21$ kg m^{-3}, although is almost insignificant from $\gamma^n = 28$ kg m^{-3} (about 2000 m).

Figure 3.4b represents the transport inside the rotating ring. There is a southward flow from stations 1 to 3 and a northward flow from 3 to 5 indicating the presence of an anticyclonic movement. This transport is greater in the thermocline, with 28 Sv, than in the intermediate waters which have 5 Sv.

3.3. Altimetry data

Data from altimeters are used to find the formation date and and to infer the ring radius. The signature in the ring was detected in October 2009, 5 months before the in situ sampling. Figure 3.5 shows the Surface Sea Height (SSH) between 32-40ºS and 3-24ºE for 6 consecutive months, from October 2009 to March 2010. The ring formation starts in a constriction of the Agulhas retroflection, and the ring continues moving northwestward. Maximum SSH is +1 m at the beginning of the ring formation (October 2009), and decreases to +70 cm at the time of the survey, in March 2010. Ghe ring radius in march is 140 km. With consecutive images of SSH we have inferred that the translation speed of the ring is 13 cm s^{-1} (468 m d^{-1}).

3.4. Drifters trajectories

3.4.1. Wavelet analysis

Wavelet spectrum is used to obtain the rotation period of the ring (Figure 3.8). In both drifters there is greater energy in the counterclockwise component, indicating that it is an anticyclonic ring. As described by Sangrà et al. (2005), eddies usually have cores with near-solid-body-type rotation and slowly revolving outer rings. The drifter trajectories (Figure 3.6) and wavelet spectrum (Figure 3.7) show that drifter 1 initially rotated with a shorter period, 7 days, because it was in the core of the ring while drifter 2 was closer to the periphery which rotated with a greater period (about 8 days). At late March, the eddy peak energy of drifter 1 becomes less sharp, spreading the energy to neighboring periods. This spreading indicates that the drifter reached the outer ring of the eddy characterized by a smaller and more irregular rotation. Both drifters left the eddy at the end of April.

3.4.2. Drifter trajectory analysis

The drogued drifters at 15 m depth remained inside the ring a total of 54 days. Drifters trajectories and the ring center displacement are illustrated in Fig. 3.6. Regarding the drifters trajectory, it is confined to the center of the ring. Mean trajectory inside the ring is Northeastward in both cases and with a translation speed of 4.1 cm s^{-1} (147.6 m d^{-1}) and 7.8 cm s^{-1} (280.8 m d^{-1}) for drifters1 and 2 respectively. Ring characteristics as mean trajectory, radius and period can be calculated from drifter positions (Brassington, 2010 and Grisolía-Santos et al. ,2015).

Firstly, to describe the lagrangian properties of the ring, it is substracted the ring center displacement obtained from drifter position interpolation is removed from to the whole trajectory obtaining thus the orbits around the ring center (fig 3.8). Orbits for drifter 1 show an elliptical shape with a major axis of ca. 25 km indicating that this buoy remained very close to the eddy center for most of the time, and increasing the orbit radius up to ca. 50 km for the last days diverging toward the ring periphery. It described 7 clockwise loops around the ring center being thus its mean period about 7.7 days. Otherwise, drifter 2 shows an opposite behavior since it starts closer to the ring periphery having also an elliptical orbit with a major axis of ca. 50 km for the first two weeks and converging towards the ring center afterwards. It described 6 clockwise loops around the ring center being thus its mean period about 9 days.

On the other hand, mean period calculated from drifter trajectory shows clearly the instant, day 28, the drifter 1 goes out of its primarly orbit close to the core ring that corresponds when the period becomes irregular. After that time, the period increases corresponding to its wandering to the ring periphery. (fig. 3.4). The period obtained during the first 28 days is aproximately 5 days. Difter 2 data is a bit different as this one starts further of ther core than drifter 1 and, thus, the 15 first days of data are those we have into account. This period is 8 days. After that the difters moves to the core and its period deacreases, reaching values of 5 days, similar to those of drifter 1 at day 30. Then the period increases again because the drifter is going out of the ring.

Figure 3.10 shows the mean radius of the rings calculated from drifter data. The results show the same behavior than obtained from other calculations. The mean radius for drifter 1 has a mean value of 25 km until day 28, before going out of the core. The mean radius for drifter 2 from day 1 to day 15 is of 50 km before going closer to the core ring.

4. Discussion and conclusion

In order to characterize an Agulhas ring, this study analyzes hydrographic data and surface salinity from a thermosalinometer acquired during MOC2-Austral cruise, SSH from altimetry and two NOAA drifters data. Our results show some characteristics of an

Agulhas rings summarized in table 1 (some of the values are obtained from different methods to compare).

Data from the CTD shows that the hydrographic structure of the ring extend to 2000 m depth as his baroclinic parent, the Agulhas Current (Garzoli et al., 1999). The water masses within the ring are similar to those found in other rings (van Aken et al., 2003). Its hydrographic properties differ from those of the surrounding waters only in the surface, subsurface and in the intermediate waters. Water trapped inside the ring comes from the Indian ocean: AGW in the surface and subsurface, and traces of RSW on the intermediate water, although its appearance seems to be intermittent (Garzoli et al., 1999). On the other side, we found the typical Atlantic Ocean waters, ASW and AAIW in its surroundings. Maximum geostrophic velocity 30 cm s^{-1}, indicating the location of the maximum energy. Rotating fluxes show a counterclockwise transport of 28 Sv. Thus, the anticyclonic rings shed from the Agulhas retroflection and transported to the Atlantic Ocean are important contributors to the interocean heat, salt and mass transport as pointed out by grazoli et al. (1999).

According to SSH data this ring is of long duration. It was spawned from the Agulhas retroflection in October 2009 with a maximum SSH of +100 cm at the beginning of his life time and a SSH of +70 cm after 6 months of life. Therefore it can be classified as a strong Agulhas ring according to van Aken et al. (2003).

The radius is calculated from the SSH images and from Brassington (2010) and Sangrà et al. (2005) method with drifters data, obtaining results with significant differences. From altimetry we obtain a radius of 140 km, which is the most realistic result due to the altimetry data can cover the entire ring (Biastoch and Krauss, 1999; Garzoli et al., 1999; Gordon and Haxby, 1990; Richardson, 2007). Drifters values are in the range of 25-55 km. These smaller values are not real because drifters are confined in the core ring, and therefore, do not measure the complete radius.

According to SSH and drifters trajectories, the ring displacement is northeastwards. In the calculation of translation speeds results from both data are different. We obtain greater values from the altimetry (13 cm s^{-1} or 468 m d^{-1}) than for the drifters (4.1 cm s^{-1} or 147.6 m $d^{-1}$and 7.8 cm s^{-1} or 280.8 m d^{-1} from drifter 1 and 2, respectively). Higher values in the

altimetry could be due to have more data in time with respect to drifter one: approximately 180 days versus approximately 40 days for the drifters. Furthermore, the SSH measurements start at the beginning of the ring life (October 2009), when the ring move faster, while the drifters data start in March 2010, when the ring has almost 6 month of life and thus shorter displacement.

Rotation period is obtained from wavelet analysis and from drifter trajectory decomposition. Few differences are obtained from the method and the drifter used. For drifter 1 values from both methods are smaller than for drifter 2. This is due to drifter 1 is closer to ring core than drifter 2, which even being in the core is closer to the periphery. According to the method used, values for wavelet analysis are greater because in this case we have used the values of all period while drifters are inside the ring. While in the drifter trajectory method it can be distinguished between the period of time when drifters are traveling inside the ring with a regular trajectory and when the trajectory becomes irregular the values are despise.

In summary, the described ring is a typical young one shed from the Agulhas retroflection with Indian water in the core and Atlantic water in its surroundings, a mean radius of 140 km, a translation speed of 13 cm s^{-1} (468 m d^{-1}) and a rotating period of 8 days.

5. References

Biastoch, A., Böning, C.W., Lutjeharms, J.R.E., 2008. Agulhas leakage dynamics affects decadal variability in Atlantic overturning circulation. Nature 456, 489–492. doi:10.1038/nature07426

Biastoch, A., Krauss, W., 1999. The role of mesoscale eddies in the source regions of the Agulhas current. Journal of Physical Oceanography 29, 2303–2317.

Brassington, G.B., 2010. Estimating Surface Divergence of Ocean Eddies Using Observed Trajectories from a Surface Drifting Buoy. J. Atmos. Oceanic Technol. 27, 705–720. doi:10.1175/2009JTECHO651.1

Ganachaud, A., 2003. Large-scale mass transports, water mass formation, and diffusivities estimated from World Ocean Circulation Experiment (WOCE) hydrographic data. J. Geophys. Res. 108, 3213–24. doi:10.1029/2002JC001565

Garzoli, S.L., Richardson, P.L., Duncombe Rae, C.M., Fratantoni, D.M., Goñi, G.J.,

Roubicek, A.J., 1999. Three Agulhas rings observed during the Benguela Current Experiment. Journal of Geophysical Research: Oceans 104, 20971–20985. doi:0148-0227/99/1999JC9000605

Gordon, A.L., Haxby, W.F., 1990. Agulhas eddies invade the south Atlantic: Evidence From Geosat altimeter and shipboard conductivity-temperature-depth survey. Journal of Geophysical Research: Oceans 95, 3117–3125. doi:10.1029/JC095iC03p03117

Grisolía-Santos, D., Rodríguez-Cruz, E., Sangrà, P., Martínez-Marrero, A., Cana, L., Barceló, B., 2015. Lagrangian evolution of a mid ocean anticyclonic eddy. 26th IUGG General assembly.

Hernández-Guerra, A., Pelegrí, J.L., Fraile-Nuez, E., Benítez-Barrios, V., Emelianov, M., Pérez-Hernández, M.D., Vélez-Belchí, P., 2014. Meridional overturning transports at 7.5N and 24.5N in the Atlantic Ocean during 1992–93 and 2010–11. Progress in Oceanography 128, 98–114. doi:10.1016/j.pocean.2014.08.016

McDonagh, E.L., Heywood, K.J., Meredith, M.P., 1999. On the structure, paths, and fluxes associated with Agulhas rings. Journal of Geophysical Research: Oceans 104, 21007–21020. doi:0148-0227/99/1998JC9001315

Rahmstorf, S., England, M.H., 1997. Influence of Southern Hemisphere winds on North Atlantic Deep Water flow. Journal of Physical Oceanography 27, 2040–2054.

Richardson, P.L., 2007. Agulhas leakage into the Atlantic estimated with subsurface floats and surface drifters. Deep Sea Research Part I: Oceanographic Research Papers 54, 1361–1389. doi:10.1016/j.dsr.2007.04.010

Richardson, P.L., Lutjeharms, J.R.E., Boebel, O., 2003. Introduction to the "Inter-ocean exchange around southern Africa." Deep Sea Research Part II: Topical Studies in Oceanography 50, 1–12. doi:10.1016/S0967-0645(02)00376-4

Sangrà, P., Pelegrí, J.L., Hernández-Guerra, A., Arregui, I., Martín, J.M., Marrero-Díaz, A., Martínez, A., Ratsimandresy, A.W., Rodríguez-Santana, A., 2005. Life history of an anticyclonic eddy. Journal of Geophysical Research C: Oceans 110, 1–19. doi:10.1029/2004JC002526

Thomson, R.E., Emery, W.J., 2014. Data Analysis Methods in Physical Oceanography: Third Edition, Data Analysis Methods in Physical Oceanography: Third Edition.

Toggweiler, J.R., Samuels, B., 1995. Effect of Drake Passage on the global thermohaline circulation. Deep Sea Research Part I: Oceanographic Research Papers 42, 477–500. doi:10.1016/0967-0637(95)00012-U

Torrence, C., Compo, G.P., 1998. A Practical Guide to Wavelet Analysis. Bulletin of the

American Meteorological Society 79, 61–78.

van Aken, H.M., van Veldhoven, A.K., Veth, C., de Ruijter, W.P.M., van Leeuwen, P.J., Drijfhout, S.S., Whittle, C.P., Rouault, M., 2003. Observations of a young Agulhas ring, Astrid, during MARE in March 2000. Deep Sea Research Part II: Topical Studies in Oceanography 50, 167–195. doi:10.1016/S0967-0645(02)00383-1

List of tables

Table 1: Ring characteristics calculated from the different data sets used in this work

	CTD	SSH	DRIFTER1	DRIFTER 2
Depth (m)	2000	-	-	-
Radius (km)	-	140	20	55
Translation speed (cm s^{-1})	-	13	4.1	7.8
Transport (Sv)	28	-	-	-
Geostrophic velocity (cm s^{-1})	30	-	-	-
Period (days) from wavelet	-	-	7	8
Period (days) from orbits			5	8
Number of loops	-	-	7	6

List of Figures

Figure 3.7: Rotary wavelet power spectrum for both drifters. A) and b) are the clockwise and counterclockwise directions respectively for drifter 1. C) and d) are the clockwise and counterclockwise directions respectively for drifter 2. The black line is the cone of influence, where edge effects become important Warm colors indicate greater energy White dashed line indicates when the drifters exits out of the ring. y axis is in power of 2.

Figure 3.8: Orbits of the drifters without the mean trajectory. a) drifter 1 and b) drifter 2. The axes are in kilometers.

Figure 3.9: Time series of the period in days for both drifters. Green line drifter 1 and red one drifter 2.

Figure 3.10: Ring mean radius (km) calculated from the drifters trajectories. Green drifter 1 and red drifter 2.

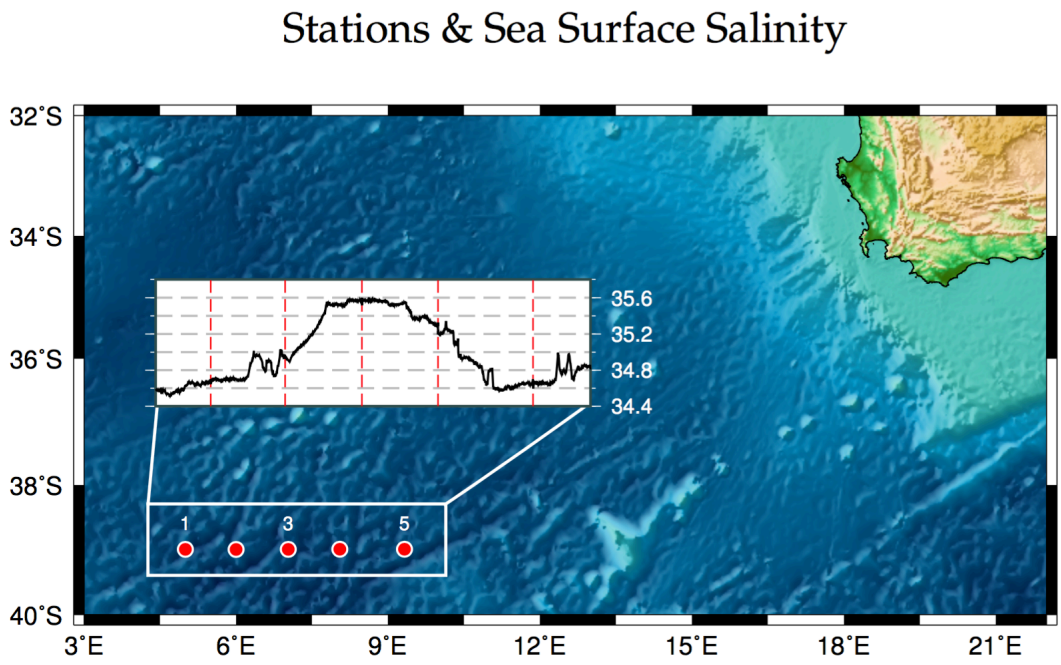

Figure 2.1: CTD station location on the studied ring and sea surface salinity indicating the presence of the ring. Red dashed lines in the inner plot show the location of the hydrographic stations.

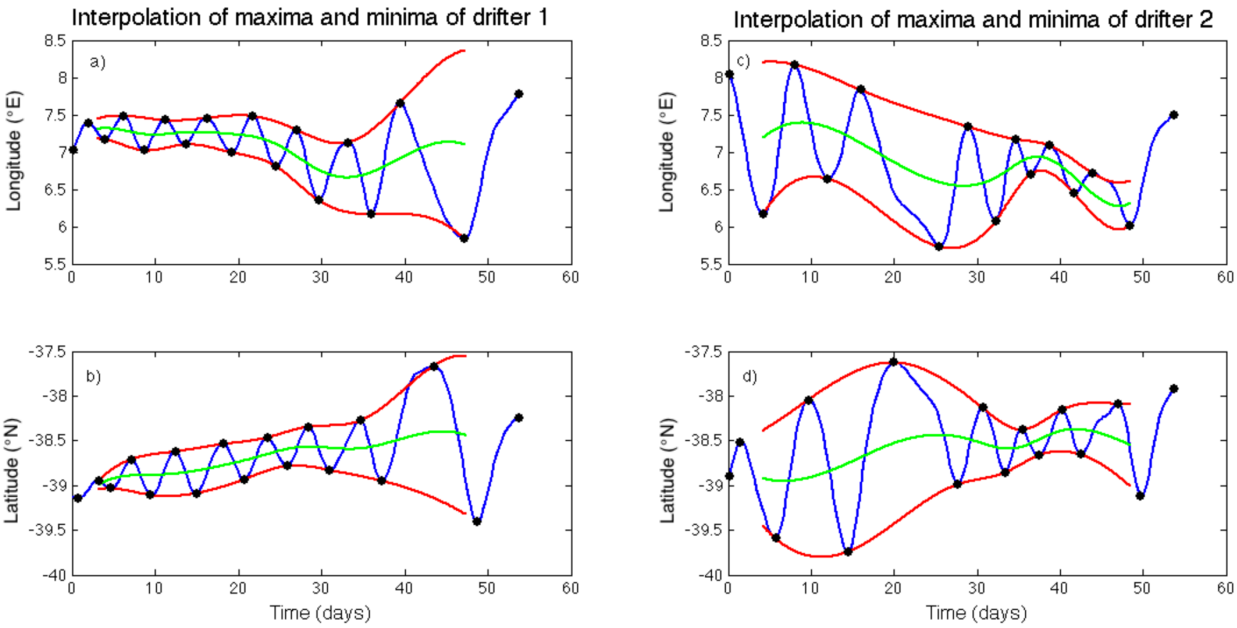

Figure 2.2: Time series of (a) longitude and (b) latitude positions of drifter 1. black circles represent the extreme that are interpolated using cubic splines (red lines) and green line show the ring center trajectory. (c), (d) as in (a), (b) but for drifter 2.

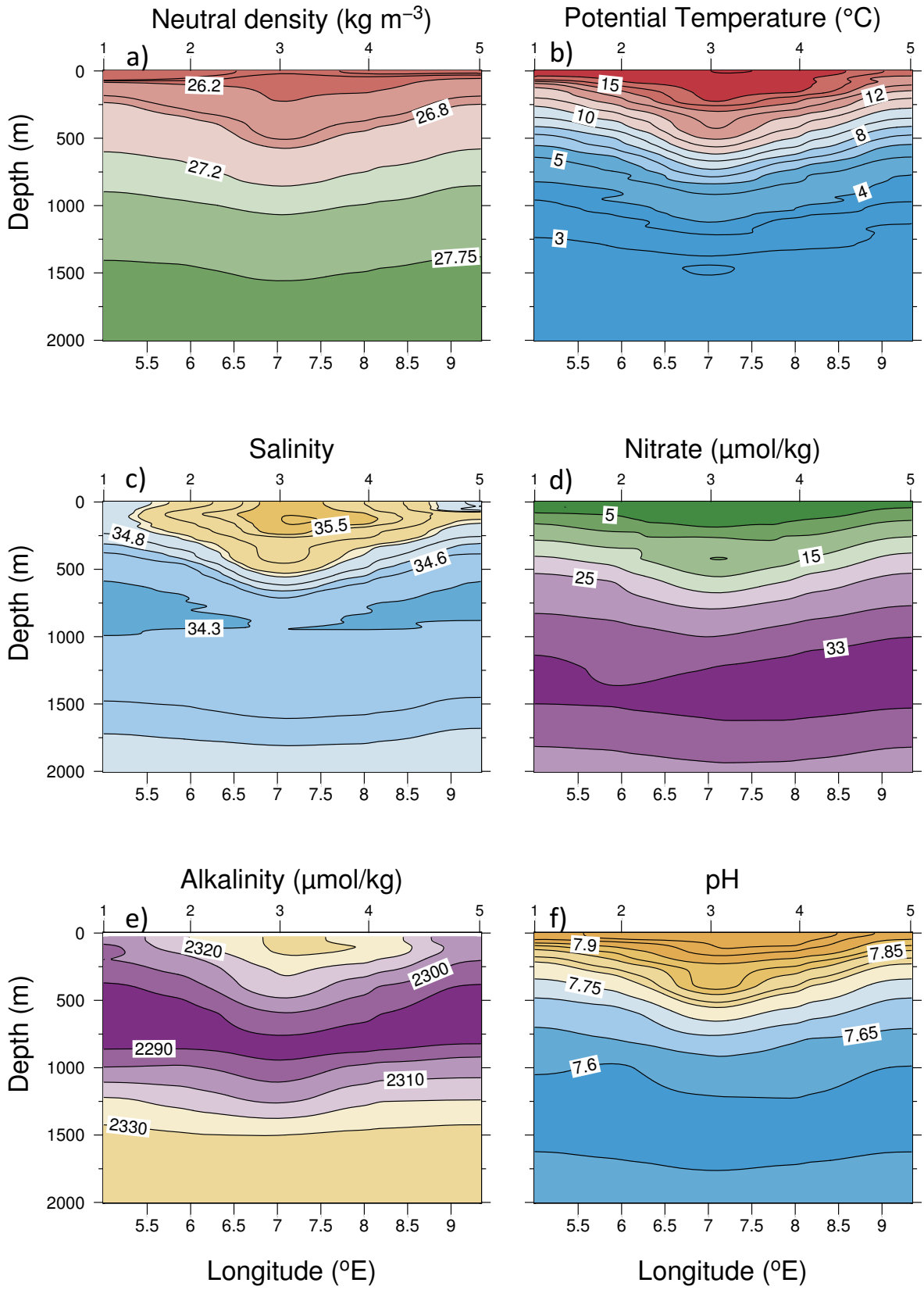

Figure 3.1: Vertical sections of a) neutral density (γ^n), b) potential temperature, c) salinity, d) nitrates, e) alkalinity and f) pH.

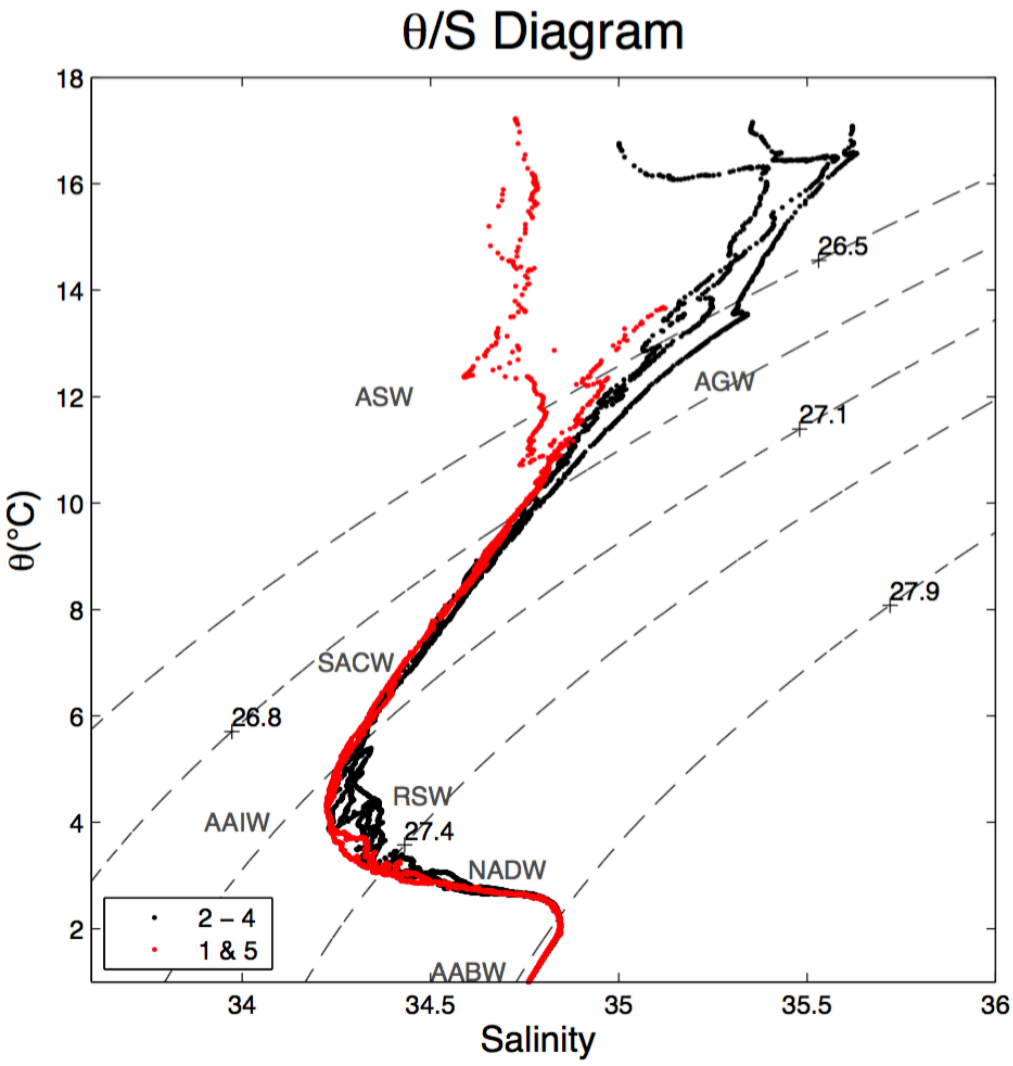

Figure 3.2: θ/S diagram to identify water masses in the Agulhas ring. Red dots represent stations 1 and 5, and black dots represent stations from 2 to 4. The masses identified are: Atlantic Surface Water (ASW), Agulhas Water (AGW), South Indian Central Water (SICW), South Atlantic Central Water (SACW), Red Sea Water (RSW), Antarctic Intermediate Water (AAIW), Antarctic Bottom Water (AABW) and North Atlantic Deep Water (NADW).

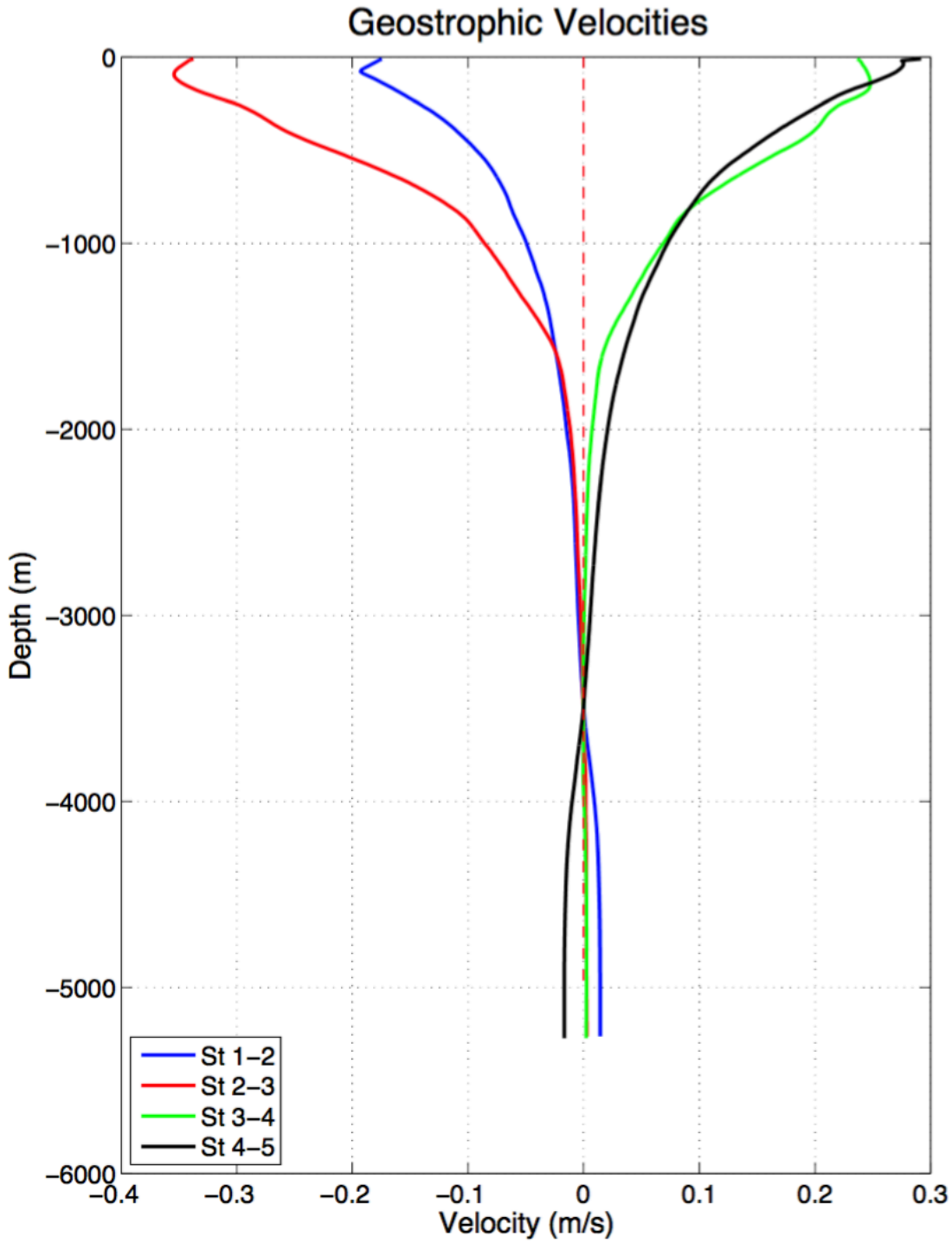

Figure 3.3: Geostrophic velocity as function of depth by pair stations. Blue for 1-2, red for 2-3, green for 3-4 and black for 4-5.

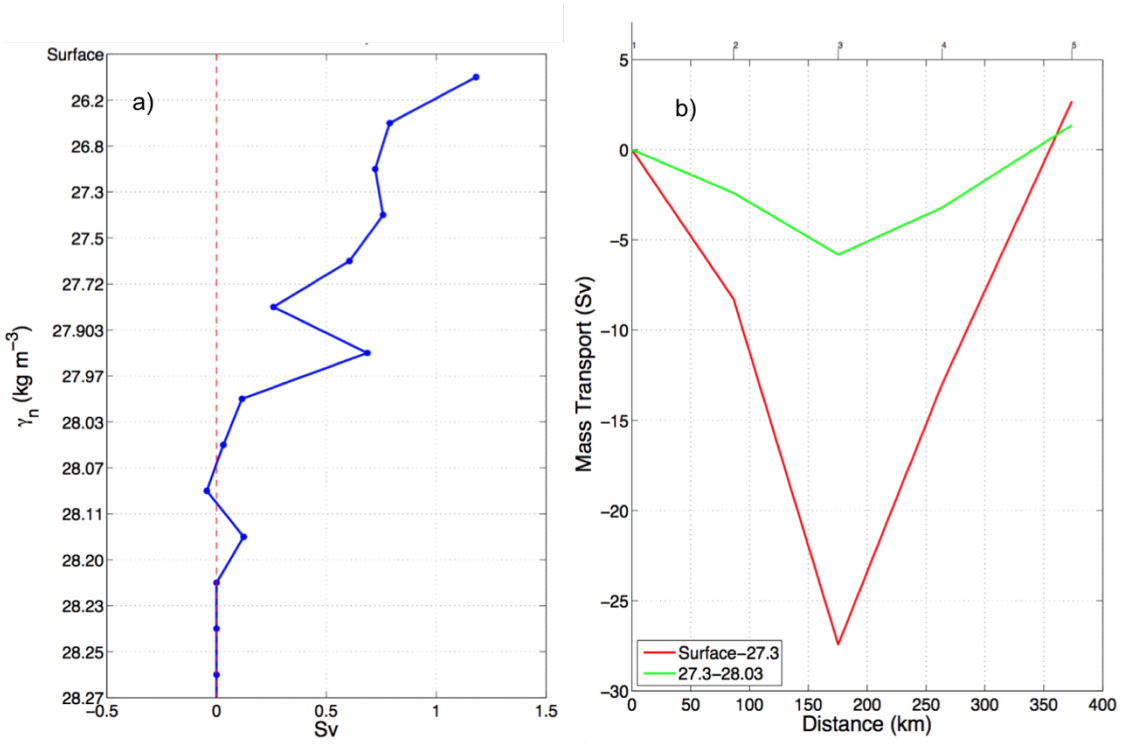

Figure 3.4: Mass transport (Sv). a) integrated mass transport for the transect per density layer. b) Accumulated geostrophic mass transport for surface (red) and intermediate (green) layers. Positive/negative values stand for northward/southward flows.

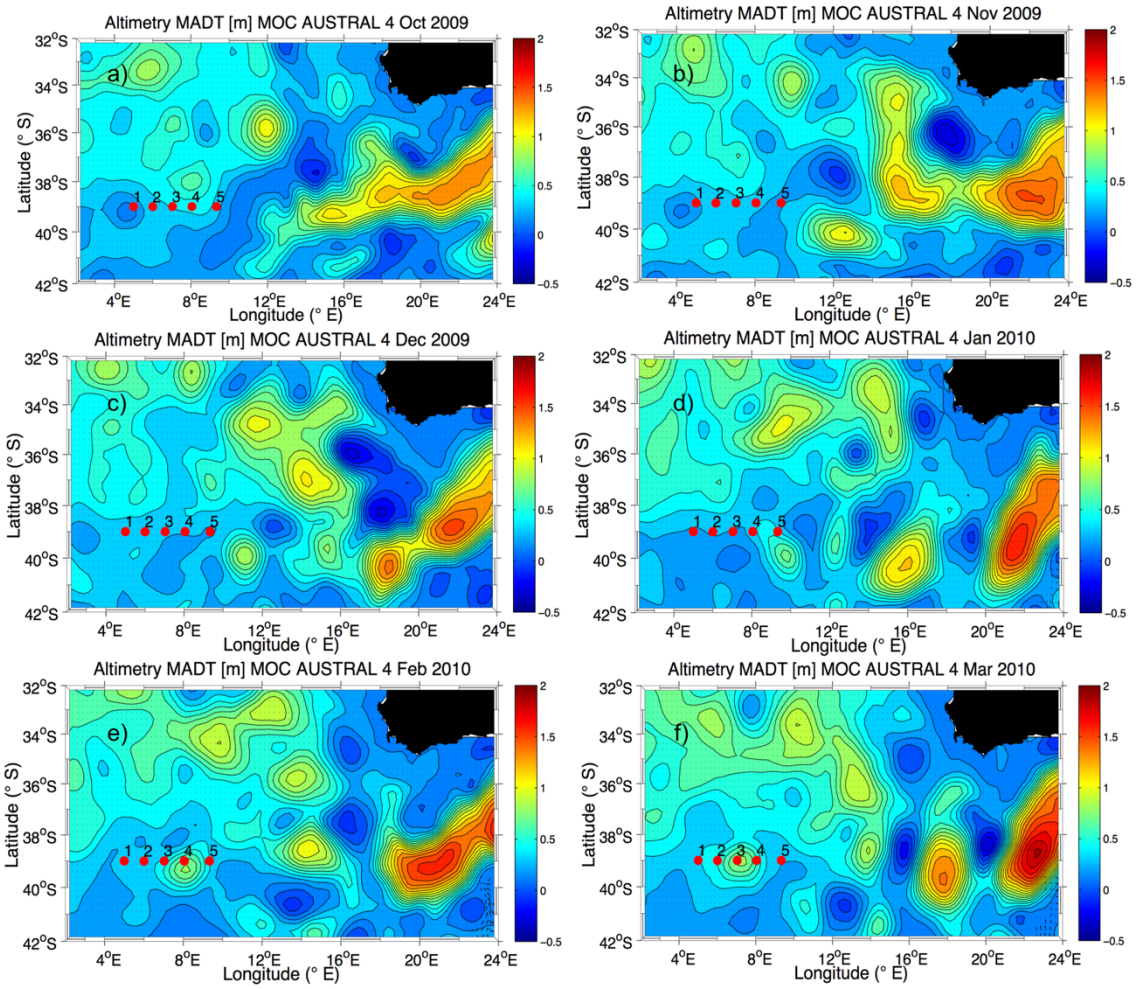

Figure 3.5: SSH images of the formation of the study ring until the survey a) October 2009, b) November 2009, c) December 2009, d) January 2010, e) February 2010 and f) March 2010 (survey dates). Red dots represent the stations during the survey.

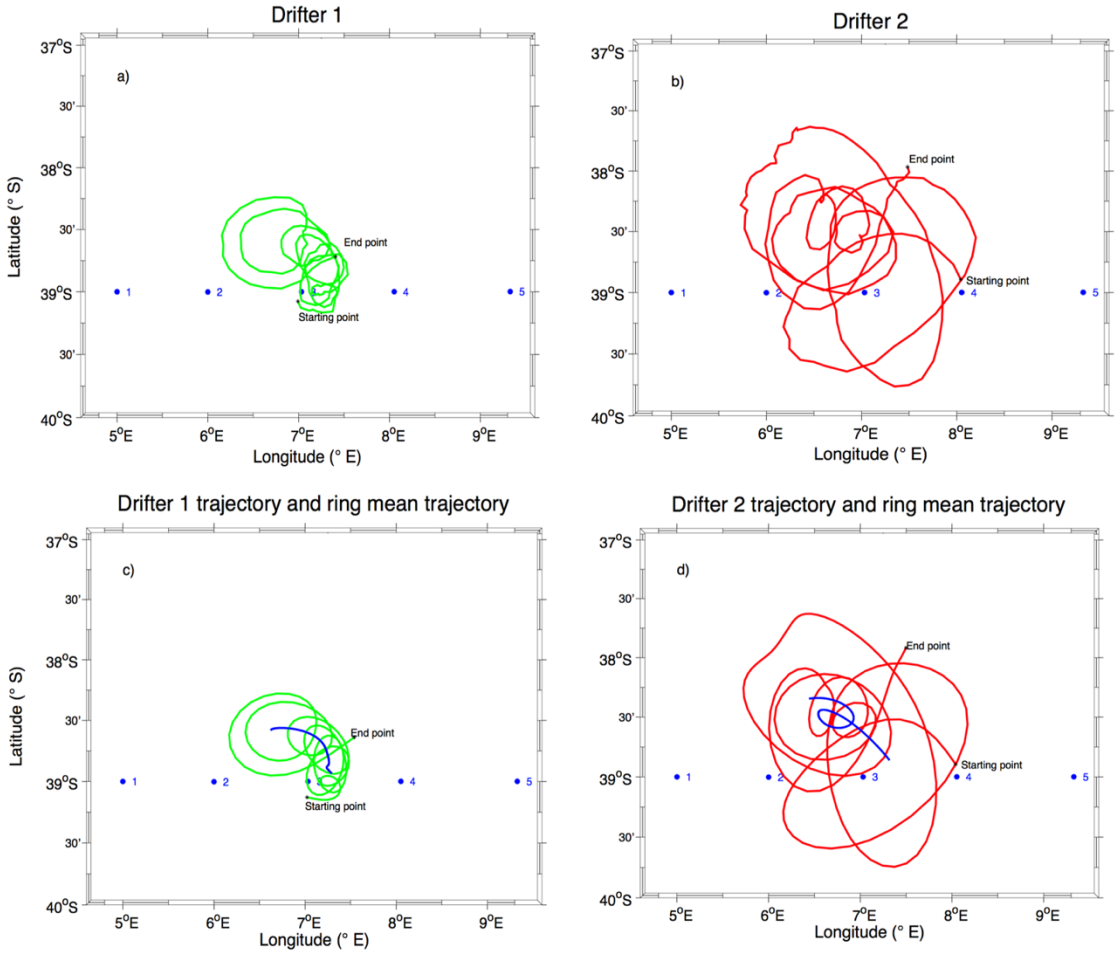

Figure 3.6: Drifters trajectories for a) drifter 1 and b) drifter 2. Blue dots are the hydrographic stations position with their corresponding number. (c) and (d) are the trajectories filtered with a low-pass butterworth filter and the ring mean trajectory (blue) for drifters 1 and 2, respectively

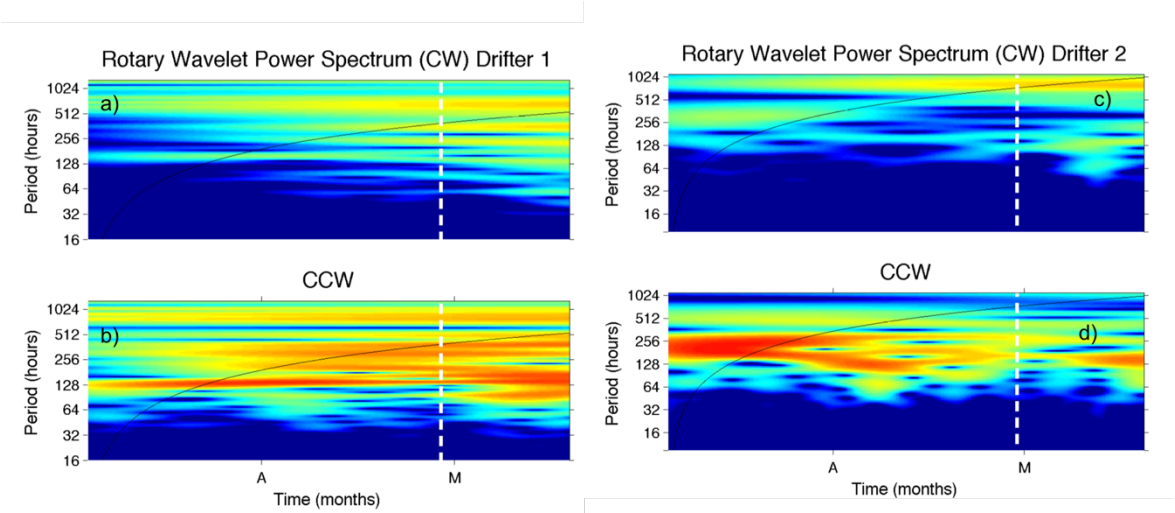

Figure 3.7: Rotary wavelet power spectrum for both drifters. a) and b) are the clockwise and counterclockwise components respectively for drifter 1. c) and d) are the clockwise and counterclockwise components respectively for drifter 2. The black line is the cone of influence, where edge effects become important. Warm colors indicate greater energy. The white dashed line indicates when the drifters exits out of the ring.

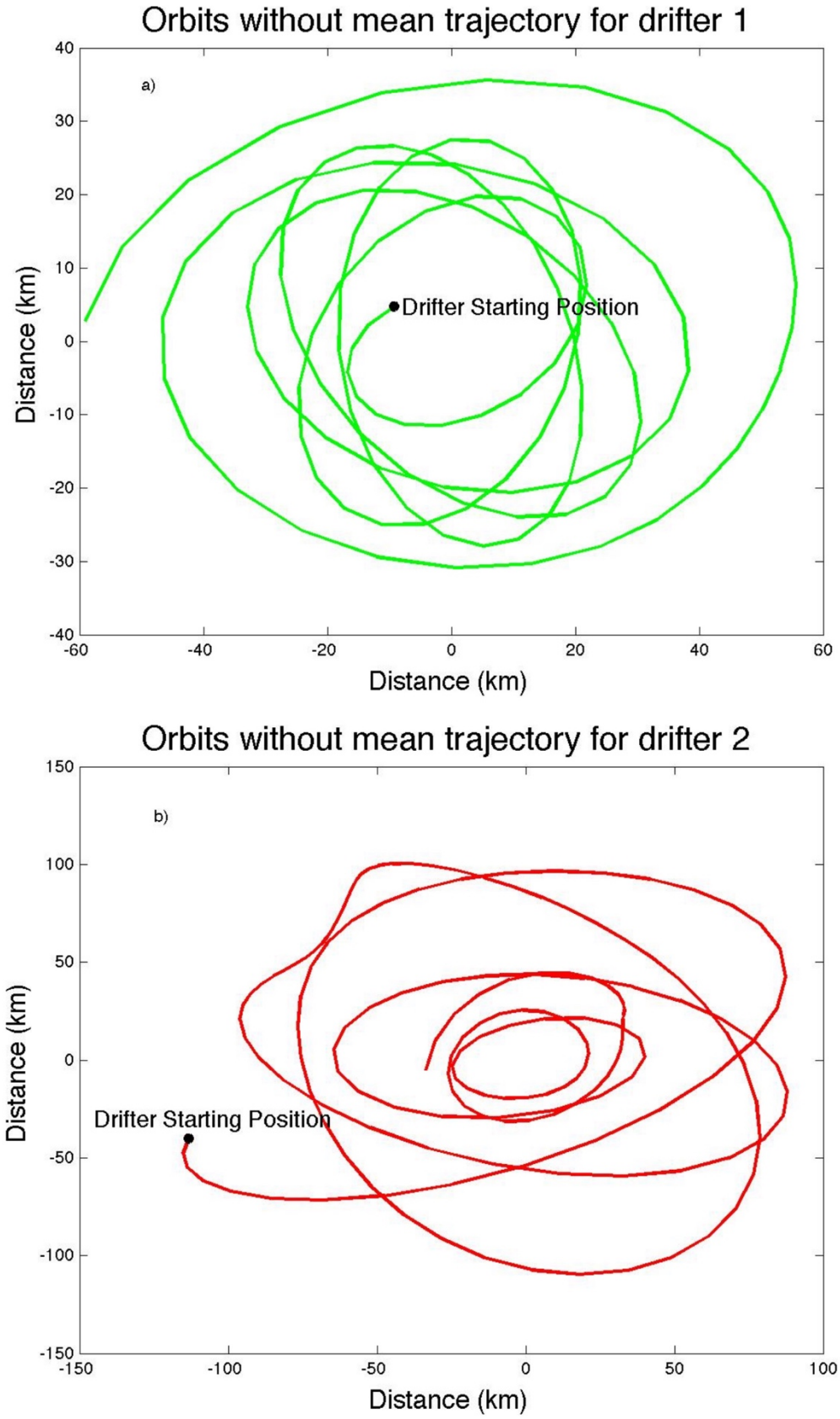

Figure 3.8: Orbits of the drifters without the mean trajectory. a) drifter 1 and b) drifter 2. The axes are in kilometers.

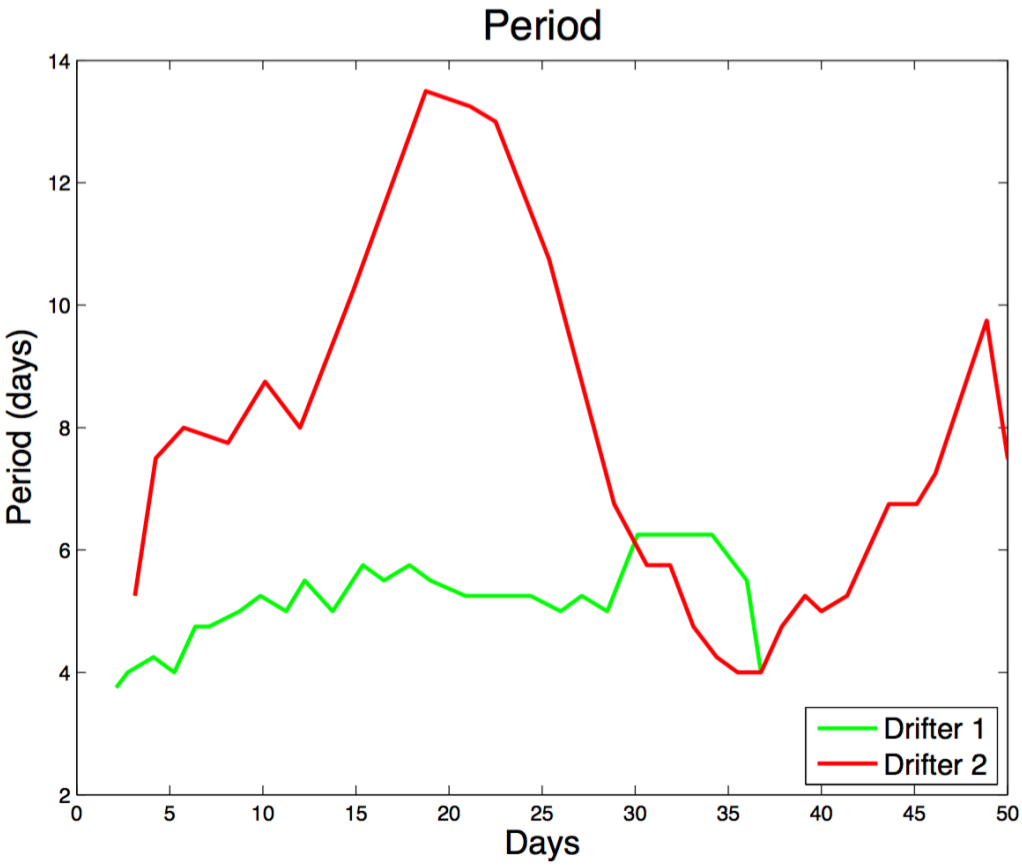

Figure 3.9: Time series of the period in days for both drifters. Green line drifter 1 and red one drifter 2.

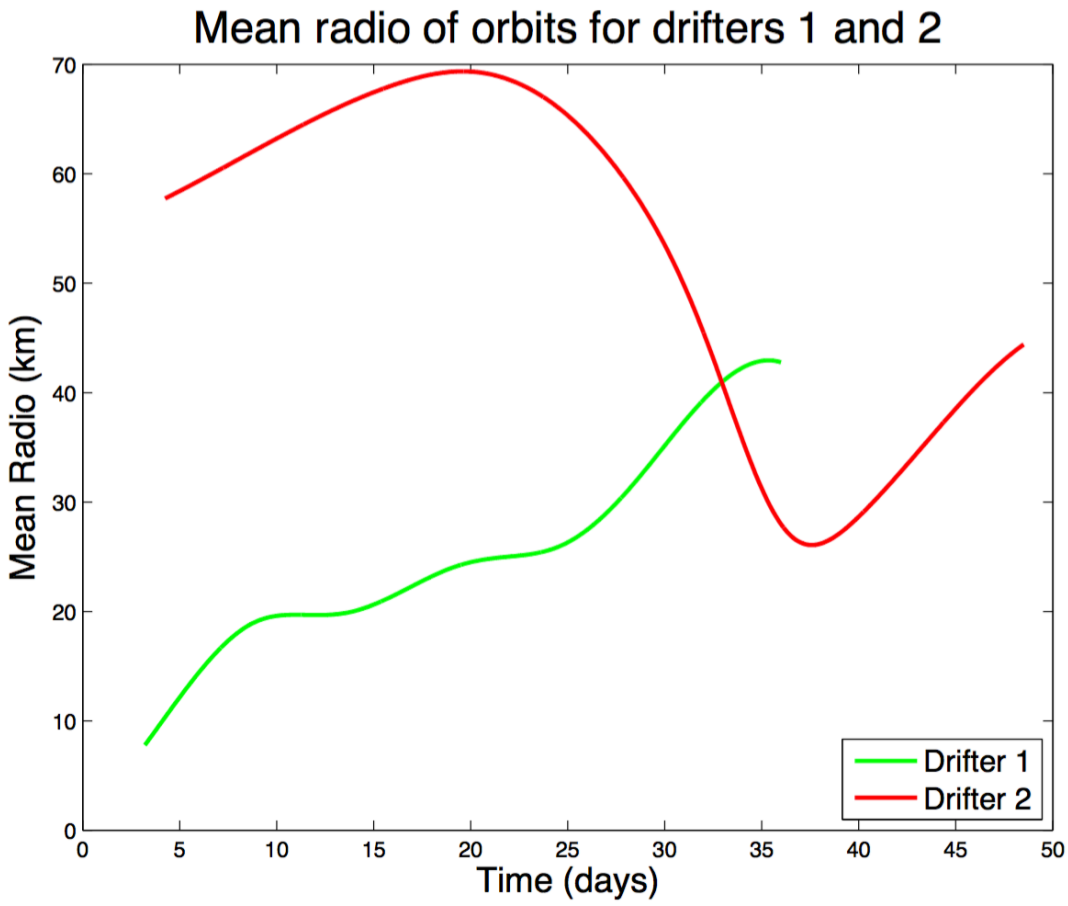

Figure 3.10: Ring mean radius (km) calculated from the drifters trajectories. Green drifter 1 and red drifter 2